Earth Planets Space, **59**, 157–164, 2007

Atmospheric stability at 90 km, 78°N, 16°E

C. M. Hall[1], T. Aso[2], and M. Tsutsumi[2]

[1]*Tromsø Geophysical Observatory, Norway*
[2]*National Institute of Polar Research, Japan*

(Received February 21, 2006; Revised October 9, 2006; Accepted October 10, 2006; Online published March 23, 2007)

We employ observations obtained from a meteor wind radar to derive ambipolar diffusion coefficients, neutral temperatures, temperature gradients and, subsequently, Brunt-Väisälä frequencies at an altitude of 90 km over Svalbard (78°N, 16°E). The derived values showed a good agreement with independent measurements at each step of the analysis. Current atmospheric models are based on sparse data obtained at such high latitude, so these results represent a viable alternative for incorporating in subsequent studies of atmospheric dynamics, particularly if the derived monthly variabilities are included. The Brunt-Väisälä frequencies are then combined with wind shear measurements to estimate horizontally averaged gradient Richardson Numbers (Ri). We find Ri to be consistently larger in summer than winter due to wind shears being similarly larger in winter and augmented by the inverse seasonal variation in Brunt-Väisälä frequency. These seasonal variations result in Ri indicative of dynamic stability in summer and instability in winter. The variabilities in wind shear and Brunt-Väisälä frequency are then included to—albeit more qualitatively—illustrate the distribution between stability and static and dynamic instabilities as a function of season, using a novel portrayal pioneered by Zink and Vincent (*J. Geophys. Res.*, **109**, doi:10.1029/2003JD003992, 2004). The resulting picture is discussed in the framework of current conceptions of distribution of turbulent energy dissipation with height and season and of current opinion of the mesopause structure at 78°N.

Key words: Mesosphere, stability, Brunt-Väisälä frequency, Arctic, meteor radar.

1. Introduction

A common prerequisite for the quantitative study of gravity waves and turbulence is knowledge of the Brunt-Väisälä, or buoyancy frequency. For upper atmosphere studies, this parameter is usually derived from some model since obtaining an instantaneous temperature profile is a non-trivial, indeed, on occasion insurmountable, task. Invariably, Brunt-Väisälä frequencies derived from models are well-behaved, varying smoothly in altitude and time; as discussed by Zink and Vincent (2004), however, this is rarely the case in reality as, for example, gravity waves (GWs), and in particular propagating across regimes of near adiabatic lapse rates, can incite regions of convective instability (negative Brunt-Väisälä frequency). An in-depth treatise on GW dynamics in the middle atmosphere has been given by Fritts and Alexander (2003) and this and many references therein provide an invaluable background for these concepts. While it is easy to appreciate the shortcomings of Brunt-Väisälä frequencies derived from models, even a lidar measurement from a rocket launching facility can yield a temperature profile unrepresentative of a payload trajectory say half a GW horizontal wavelength away. While, in this study, we do not pretend to solve such problems, local temperature measurements obtained by meteor wind radar (MWR) are used to estimate monthly Brunt-Väisälä frequencies that offer an alternative to those derived from models hitherto based on sparse high latitude data.

The Nippon/Norway Svalbard Meteor Radar (NSMR) meteor wind radar (MWR) situated at 78°N, 16°E on Spitsbergen has been operating since the spring of 2001. With a transmitting frequency of 31 MHz, the preferred height for meteor train echoes is 90 km and virtually all echoes are seen within a zenith angle of 70°. The system provides vector horizontal winds and ambipolar diffusion coefficients averaged over the field of view (an important consideration) with a nominal time resolution of 30 min and a height resolution of 1 km. Values are truly independent at resolutions of 60 min and 2 km due to use of a weighting function in the analysis procedure.

Determinations of neutral temperatures in the upper mesosphere using MWR data have been discussed in depth by Holdsworth *et al.* (2006) and here their philosophy is applied to data obtained from the NSMR. Temperatures at 90 km have been derived from this instrument earlier (Hall *et al.*, 2004) but only as a pilot study, and improved results from Hall *et al.* (2006) are used here, primarily due to the employment of a more suitable pressure model (Holdsworth *et al.*, 2006; Lübken, 1999; Lübken and von Zahn, 1991). As earlier, we shall concentrate on an altitude of 90 km, the preferred altitude for meteor echoes for NSMR. While details of the derivation of ambipolar diffusivities, D, of ions in the meteor trails have been discussed earlier (by, for example, Holdsworth *et al.*, 2006), it is important to examine the subsequent derivation of neutral temperature, T:

$$D = 6.39 \times 10^{-2} \frac{K_0 T^2}{P} \qquad (1)$$

where P is the pressure (in Pa) and K_0 (in $m^2\ V^{-1}\ s^{-1}$) is the zero field mobility. We have attributed 2.4×10^{-4} to K_0 following Cervera and Reid (2000). From the above expression we see the necessity for pressure data and these have been obtained from the mass densities and temperatures published by Lübken (1999) and Lübken and von Zahn (1991) as Holdsworth *et al.* (2006) did, and then since we shall be deriving monthly averages, interpolating to a 12-month grid.

Rearranging Eq. (1) and differentiating with respect to height, z, we arrive at:

$$\frac{dT}{dz} = \frac{T}{2}\left(\frac{1}{P}\frac{dP}{dz} + \frac{1}{D}\frac{dD}{dz}\right) \tag{2}$$

and, thereafter, the temperature and temperature gradient may be used to determine the Brunt-Väisälä frequency ω_B (rad^{-1}) from

$$\omega_B = \sqrt{\left(\frac{dT}{dz} + \frac{g}{C_p}\right)\frac{g}{T}} \tag{3}$$

in which g is the acceleration due to gravity and C_p is the specific heat of dry air at constant pressure. We take $g = 9.54\ ms^{-2}$ (90 km altitude) and $C_p = 1009\ J\ kg^{-1}\ K^{-1}$ (for a typical temperature of 170 K).

The distribution of turbulent energy dissipation with season and altitude through the mesosphere has been common knowledge for at least two decades (e.g. Hall *et al.*, 1999 and references therein): there is turbulence more or less throughout the mesosphere during winter, whereas in summer almost all energy dissipation occurs in the "steep beach" region immediately above the mesopause (e.g. McIntyre, 1989) with little turbulence in the mesosphere itself. Since we do not yet have a complete understanding of phenomena occurring in the mesopause region, it is important to study transport processes for trace gases, energy and momentum and, therefore, gravity waves (GW) and the production of turbulence (Fritts and Alexander, 2003; McIntyre, 1989). Consider the Richardson Number, Ri (e.g. Kundu, 1990), where

$$Ri = \frac{\omega_B^2}{(d\mathbf{U}/dz)^2} \tag{4}$$

in which ω_B is the buoyancy or Brunt-Väisälä frequency, $\mathbf{U}$ is the horizontal wind velocity and z is height such that the denominator is therefore the square of the magnitude of the vertical gradient of horizontal wind. We have used ω_B rather than N to denote the Brunt-Väisälä frequency as a reminder that this quantity is in $radian^{-1}$ as opposed to Hertz. (Kundu, 1990). When Ri is negative the atmosphere is convectively unstable (ω_B is imaginary); when $0 < Ri < 0.25$ there is a dynamic instability and turbulence may be expected; existing turbulence may just be maintained when $Ri = 0.4$; the atmosphere will be stable for $Ri > 1$. These various conditions have been much discussed in the literature and should not be taken as de facto (e.g. Weinstock, 1978; Roper and Brosnahan, 1997). Earlier, Hall *et al.* (2002) evaluated Ri in the upper mesosphere at 78°N, 16°E in a pilot study to assess the seasonal variation in dynamic instability and we shall extend this approach here.

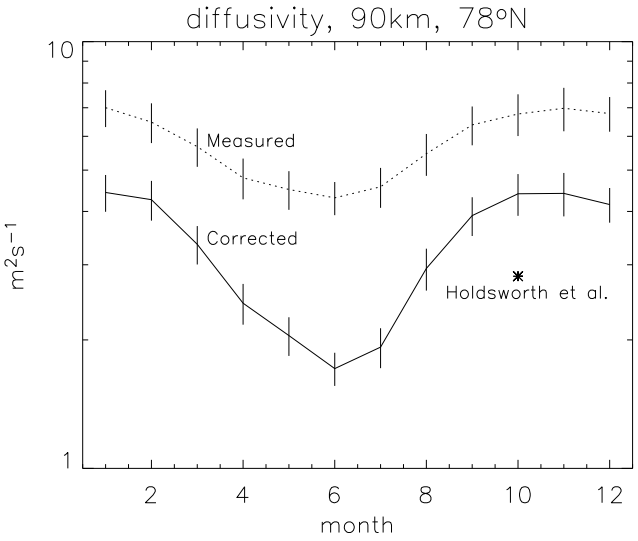

Fig. 1. Monthly averages of ambipolar diffusion coefficient at 90 km, 78°N, 16°E derived from measurements between 2001 and 2005. The solid line, annotated "corrected", has been obtained by calibrating the measured values (dashed line) by optical methods. The April 2004 determination for 90 km, 69°S by Holdsworth *et al.* (2006) has been included at October.

2. Brunt-Väisälä Frequency: Results

To summarize, in order to estimate the Brunt-Väisälä frequency we need to obtain the temperature and temperature gradient representative of 90 km; in order to determine these we need to know the atmospheric pressure and its gradient and to measure the ambipolar diffusion coefficient and its gradient. Building on the exploratory study by Hall *et al.* (2004), Hall *et al.* (2006) determined monthly temperatures for 78°N at an altitude of 90 km, the prime improvement being the use of 70°N pressures derived from the Lübken (1999) and Lübken and von Zahn (1991) observations and the adjustment of these to 78°N. In these studies, the MWR-derived temperatures are calibrated against simultaneous optical measurements prior to forming monthly averages. Here we use the same information to calibrate ambipolar diffusion coefficients from 4 years (1433 days) of observations between 2001 and 2005 inclusive such that Eq. (1) holds. The monthly average ambipolar diffusion coefficients are shown in Fig. 1, which also includes the measured values prior to calibration according to Hall *et al.* (2006). In addition, we have included the April 2004 measurement by Holdsworth *et al.* (2006) for 69°S, plotting it at October for the northern hemisphere. It is noteworthy that this value is the same as that reported by Galligan *et al.* (2004) (90 km altitude, 43°S) who used approximately 3×10^5 echoes between 1995 and 1999, both supporting our measurement and suggesting that there is very little latitude dependence of D, at least at 90 km. Thereafter the differences between the values from 89 and 90 km are used to determine the gradients dD/dz at 89.5 km, which in turn are normalized by dividing by D, as shown in Fig. 2. To give an impression of d^2D/dz^2, the 90.5 km dD/dz is also indicated in Fig. 2. We have indicated the monthly standard deviations in Fig. 2 and stress that these should not be confused with errors. If we compute the weighted averages of the frac-

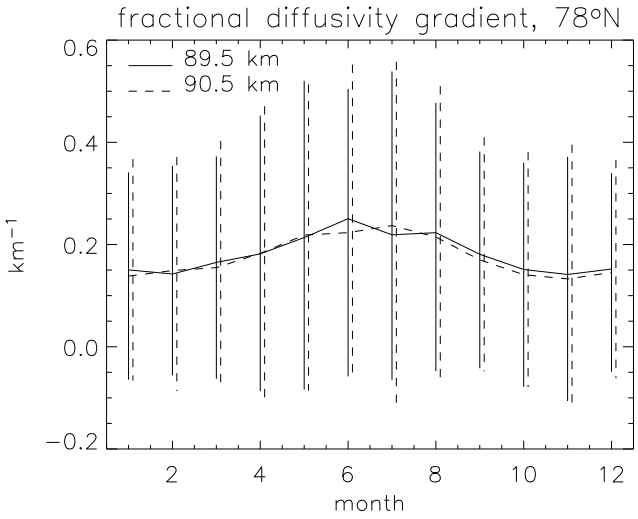

Fig. 2. Monthly averages of fractional ambipolar diffusion coefficient, $1/D \cdot dD/dz$, at 89.5 (solid line and solid standard deviation bars) and 90.5 (dashed line and dashed standard deviation bars) km, 78°N, 16°E derived from measurements between 2001 and 2005.

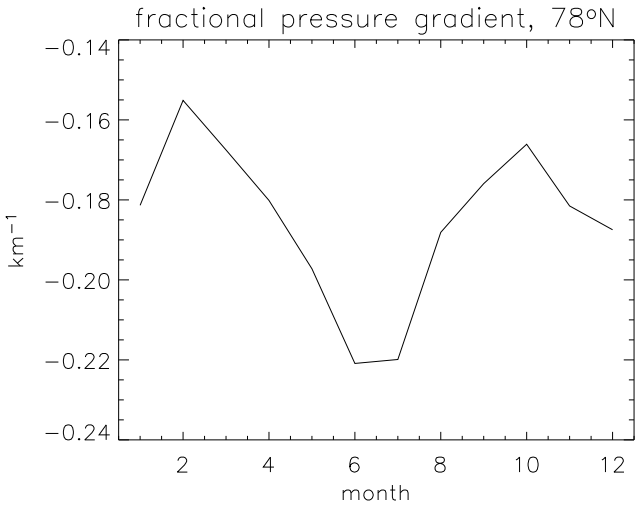

Fig. 3. Monthly fractional pressure gradients for 90 km, $1/P \cdot dP/dz$, derived from Lübken (1999) and Lübken and von Zahn (1991). Although determined from measurements at 70°N, these values are assumed to be also representative for 78°N.

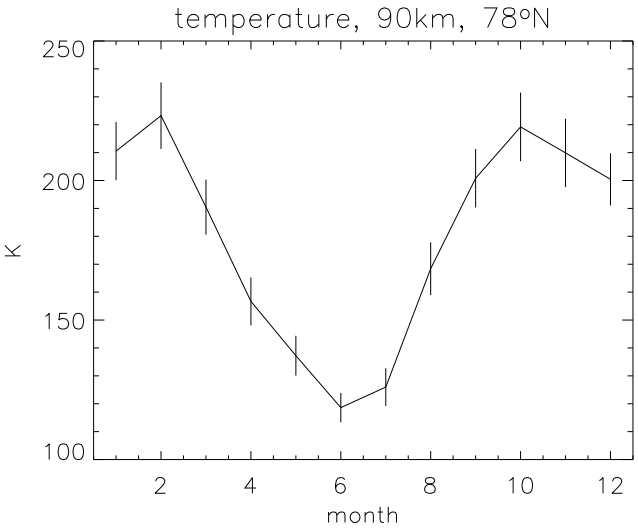

Fig. 4. Monthly temperatures for 90 km, 78°N. Uncertainties are derived from the standard deviations in averaging daily ambipolar diffusion coefficients to form monthly means.

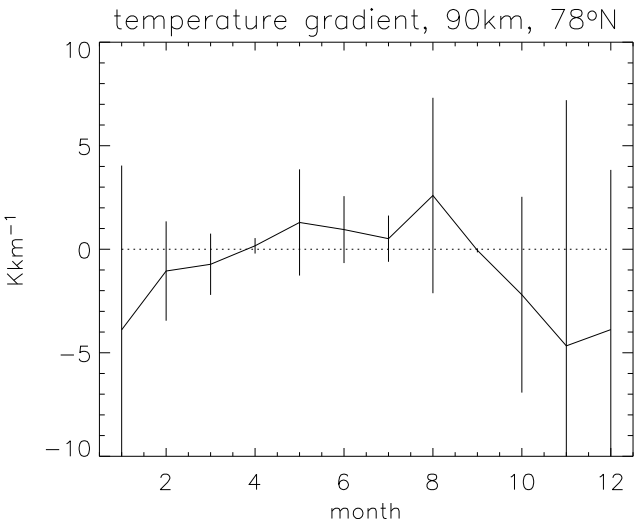

Fig. 5. Monthly temperatures gradients for 90 km, 78°N. Uncertainties are derived from the standard deviations in T, D and dD/dz. The horizontal dotted line is the demarcation between positive and negative gradients, interpreted as summer and winter mesopause states respectively.

tional diffusivity gradient for heights 88-92 km inclusive, we find that the average (over 12 months) weighted average standard deviation is then reduced to 0.11 km^{-1} for a seasonal variation little different from those shown in Fig. 2. Thus, while weighted averaging reduces the standard deviations, the seasonal variation remains.

Pressures and pressure gradients are derived from Lübken (1999) and Lübken and von Zahn (1991). Although these are derived from observations at 70°N, we have chosen not to attempt any adjustment for latitude in order to preserve consistency between pressures and gradients. We justify this by noting that Holdsworth *et al.* (2006) successfully applied these very values to MWR observations at 69°S. As for D, fractional pressure gradients, $1/P \cdot dP/dz$, are formed and these are shown in Fig. 3.

Temperatures are recalculated according to Eq. (1) and using D and P described above. Small differences between the resulting values and those found by Hall *et al.* (2006) arise from our use of unmodified pressures for 70°N and because the monthly average Ds are used to form monthly average Ts, as opposed to working with daily values (Fig. 4). Uncertainties are derived from the standard deviations in averaging daily ambipolar diffusion coefficients to form monthly means. Corresponding temperature gradients, shown in Fig. 5, are then determined according to Eq. (2) by combining these temperatures and the fractional pressure and diffusion coefficient gradients. Here, the uncertainties are indeed large; however, any concerns are reconciled somewhat when we compare the periods of positive and negative gradients with the presumed seasonal variation of the mesopause as will be discussed in the next section. In Fig. 2, we note that there is a good agreement between

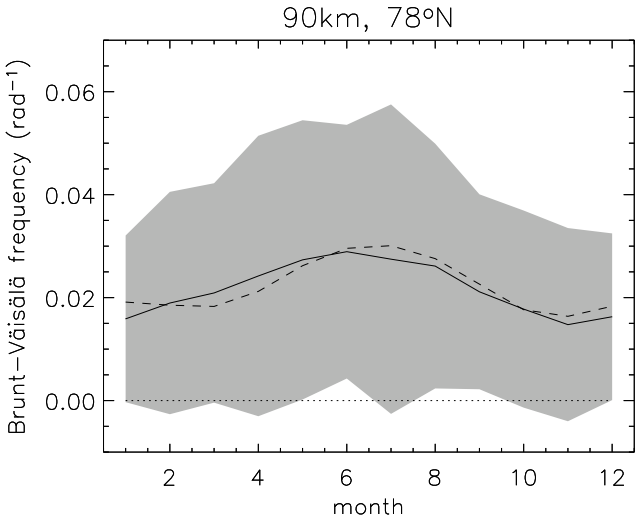

Fig. 6. Monthly average Brunt-Väisälä frequencies (rad^{-1}) for 90 km, 78°N (solid line), together with uncertainties/monthly variabilities shown by grey shading derived from uncertainties in T and dT/dz. The dashed line indicates the values obtained using NRLMSIS-00. The dotted line is the demarcation between static stability (positive values) and instability (negative values).

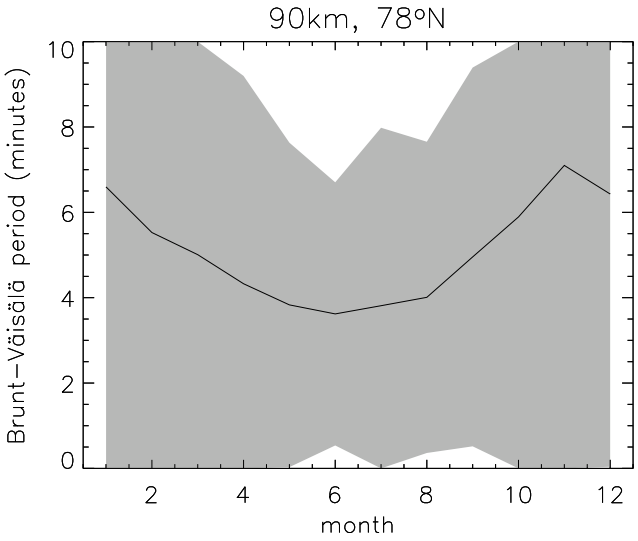

Fig. 7. The monthly average Brunt-Väisälä periods (in minutes) for 90 km, 78°N, together with uncertainties/monthly variabilities shown by grey shading, corresponding to the results in Fig. 6.

dD/dz—with the exception of June and July; thus, to improve our confidence in the subsequent summer temperature gradients, we average together the dD/dz for 89.5 and 90.5 km. Again, uncertainties are the combined standard deviations in T, D and dD/dz.

Finally, we estimate the monthly Brunt-Väisälä frequencies using Eq. (3) and, for comparison purposes, we have determined corresponding values from the NRLMSIS-00 atmosphere model (Picone *et al.*, 2002) (Fig. 6). In arriving at a set of monthly estimates of Brunt-Väisälä frequency we have attempted to minimise experimental error by day-averaging and subsequent calibration (Hall *et al.*, 2004, 2006) and then rigorously propagated standard deviations. We propose, therefore, that the uncertainties shown in Fig. 6, although seemingly large, indeed provide a verisimilitude of the monthly variability arising from intra-month wave activity affecting both the absolute temperatures and their gradients.

3. Brunt-Väisälä Frequency: Discussion

We have already commented on the plausibility of the ambipolar diffusion coefficients by citing observations from New Zealand and Antarctica; let us also address, therefore, the veracity of the resulting temperatures and gradients. Using in situ methods, Lübken and Müllemann (2003) measured July mesopause temperatures of 128 ± 6K with a mesopause altitude of 89 ± 1.5 km, in excellent agreement with Fig. 4. It should be noted that the potassium lidar which provided the 90 km summer temperatures used by Hall *et al.* (2004, 2006) to calibrate the MWR estimates also provided initial values—although at 95 km—for the derivation of Lübken's and Müllemann's (2003) results. Thus, although the two datasets are not 100% independent, our results are the average of 4 years of (almost) daily values. Lübken and Müllemann (2003) also note changes in the altitude of the mesopause, from the more well-defined summer state in July and August, just below 90 km on average, to the initially more structured winter state in September. We can see the transition to the winter state, also in September, in Fig. 5, where the temperature gradient turns negative. Interestingly, this is in contrast to the semi-empirical temperature gradient model for 70°N used by Singer *et al.* (2004) in an alternative method for determining temperatures from MWR, reflecting the differences in summer mesopause altitude and the summer-winter transitions between 70°N and 78°N.

We see from Fig. 6 that our estimates of Brunt-Väisälä frequency are in excellent agreement with the prediction of the NRLMSIS-00 model. The data input to NRLMSIS-00 at 78°N is sparse compared to, for example, that at 70°N, and the model values rely heavily on harmonic analysis; even so, the model-derived Brunt-Väisälä frequencies are highly satisfactory. On the other hand, the variability might be considered of be of greater interest than the values themselves. It is perhaps easier to appreciate this if we express the results in terms of Brunt-Väisälä periods rather than frequencies, as we have done in Fig. 7. We see that the average value lies in the region of 5 min, the "accepted" value. The summer value lies roughly between 1 and 7 min, while in winter the variability is considerable. Indeed, from Fig. 6, one can see that the 1-σ uncertainty extends to negative values on many occasions, indicating that during some proportion of the time—especially during winter—the atmosphere is statically unstable. There is an inherent difference between the results, i.e. the Brunt-Väisälä frequencies and their variabilities shown here and, for example, values derived from NRLMSIS-00. We are able to appreciate the shortness, both average (approx. 4 min) and short-term, of Brunt-Väisälä periods in the summer lower thermosphere—the "steep beach" scenario for GW breaking (e.g. McIntyre, 1989). In winter, the periods are longer (approx. 6 min), but the variability is greater, and to such an extent that convective instability is not improbable.

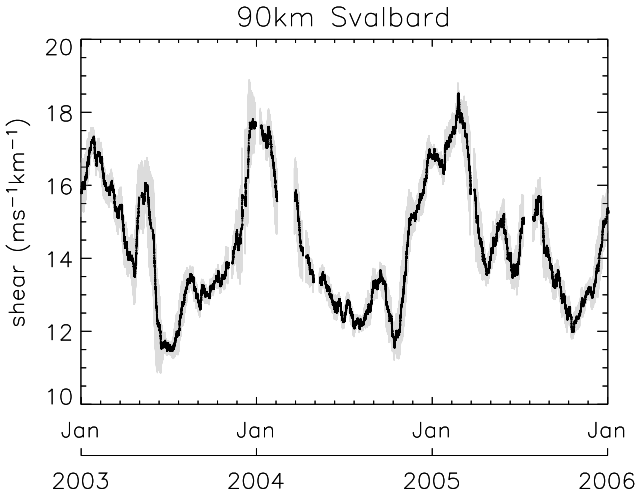

Fig. 8. Wind shears at 90 km obtained from 46,320 30-min velocity profiles from NSMR. A 1-month smoothing has been applied to produce this figure in order to reveal the consistent seasonal variation. The grey shading indicates the running standard deviation corresponding to the 1-month smoothing window.

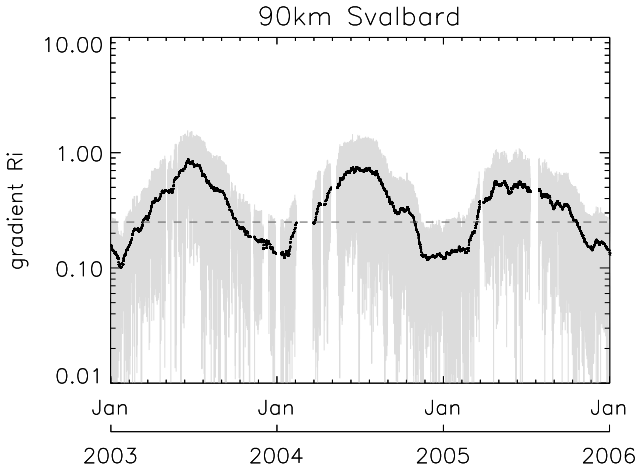

Fig. 9. Spatially averaged Richardson Numbers at 90 km obtained from 46,320 30-min velocity profiles from Fig. 8 and the monthly Brunt-Väisälä frequencies from Fig. 6. Again, a 1-month smoothing has been applied to produce this figure in order to reveal the seasonal variation. The $Ri = 0.25$ abscissa indicates the condition for dynamic instability. The grey shading indicates the day-to-day variability due to the dominating Brunt-Väisälä fluctuations.

4. Stability: Results, Caveats and Initial Interpretation

Although data are available from NSMR from as early as Spring 2001, system changes and interruptions in operation occurred during 2001 and 2002. In order to work with results from whole years, therefore, we have restricted our selection to the period 2003–2005 inclusive, which gives us a total of 46,320 30-min velocity profiles. Initially, we determine the wind shears $|d\mathbf{U}/dz|$ at 90 km for each available time-step. These are shown in Fig. 8. after applying a 1-month smoothing in order to reveal the seasonal variation; the data are clearly consistent from year to year. Thereafter, we determine Ri according to Eq. (4). at the same time-resolution using ω_B from the appropriate month. The use of Brunt-Väisälä frequencies at the time-resolution of the wind shear was found to be not viable because of short-term fluctuations in the gradient of the ambipolar diffusion coefficient required for obtaining the temperature gradient. Although the resolutions of 30 min and 1 km may sound good for MWR data, wind shears and therefore Ri are indeed averaged over a substantial horizontal area. Just how large this area is depends on the spatial distribution of the meteor trail echoes obtained within each 30-min timeslot; 100 events per 30-min is typical for NSMR, but it is unlikely that these will be distributed uniformly in azimuth. Thus, "spatially averaged Ri" is a better expression for the values we obtain, although—for convenience—we shall simply refer to "Ri" when in the context of our observations. While "bulk Ri" may sound appropriate, formally this is a quantity founded on spatial and velocity scales (Kundu, 1990) similar to the formulation of the Froude Number. These spatially averaged Ri are shown in Fig. 9, again after 1-month smoothing, to reveal seasonal spatially averaged Ri variation.

The seasonal variations shown in Figs. 8 and 9 are particularly striking, and it is important to note that the seasonal variations in ω_B and $|d\mathbf{U}/dz|$ complement each other. It would be justifiable to question the veracity of a seasonal

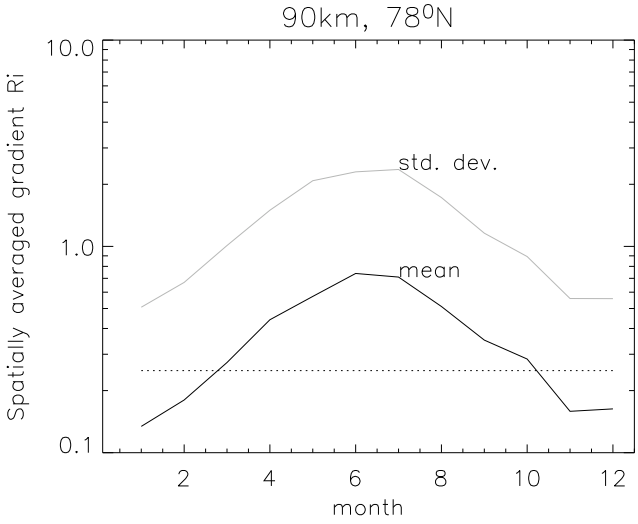

Fig. 10. Seasonal variation of spatially averaged Richardson Numbers at 90 km from monthly averages and standard deviations of the 30-min resolution data shown in Fig. 9. The dashed abscissa at $Ri = 0.25$ indicates the demarcation between turbulence generation and maintenance.

variation in Ri had the wind shear been constant with season within the instrumental uncertainty and had ω_B been obtained from a model atmosphere. In this case, however, the seasonal variation in spatially averaged Ri is incontestable and is not a manifestation of a model ω_B. Creating monthly averages from the 30 min- resolution data we can formulate a monthly climatology of Ri along with its monthly variability (as opposed to error), as shown now in Fig. 10. Here the standard deviations are derived rigorously by combining those from both in ω_B and $|d\mathbf{U}/dz|$, and the values are shown as a separate curve in the figure rather than vertical bars. The Ri $= 0.25$ demarcation between turbulent generation and maintenance is shown as a dashed abscissa. Clearly, the atmosphere (at 90 km) is, on average, more dynamically stable during the summer, although

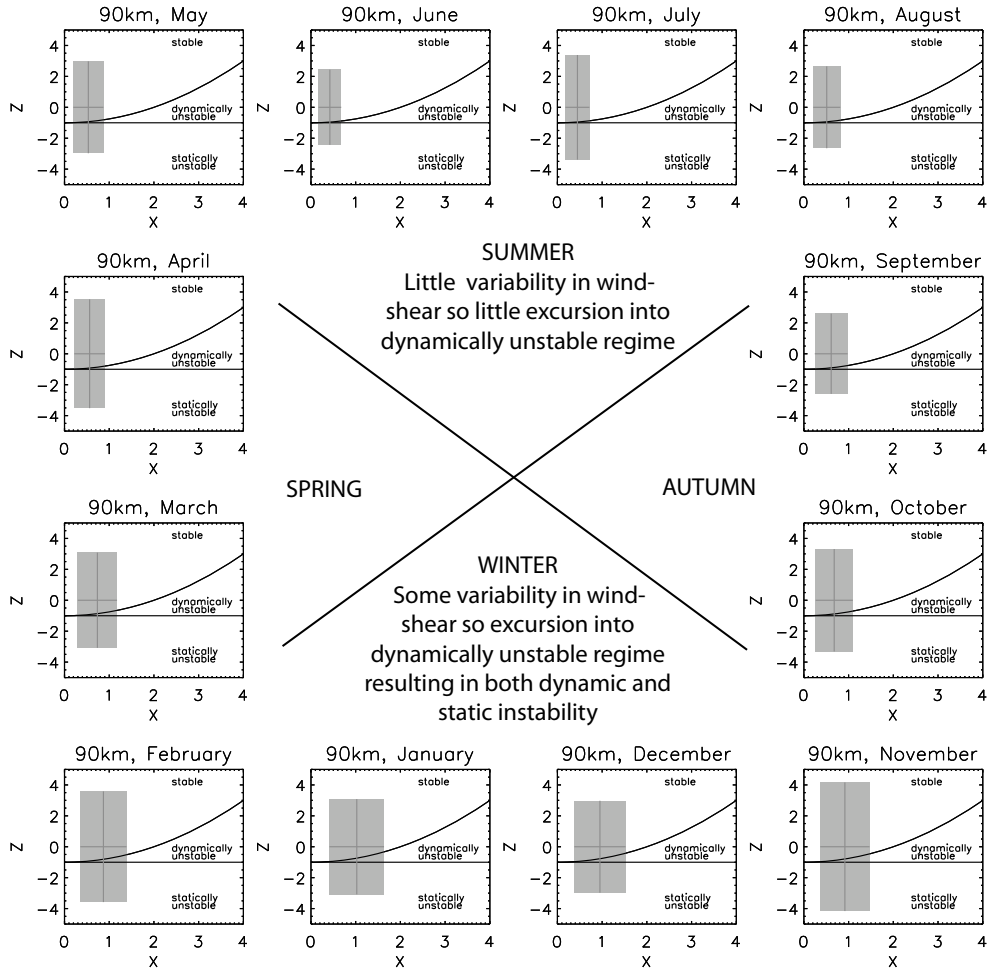

Fig. 11. Pictorial representation of monthly variation of distribution dynamic and static instabilities at 90 km, 78°N, 16°E. The year progresses clockwise with summer at the top. The width and height of the shaded rectangle indicate the degree of fluctuation of Richardson Number and Brunt-Väisälä frequency respectively, while a rightward (high X) shift indicates lower average Richardson Number.

the standard deviations suggest that dynamic or even static instability can occur at any time of the year. Further interpretation of the seasonal variation of Ri is best done by taking the mesopause altitude into consideration. Lübken and von Zahn (1991) and Lübken (1999) have demonstrated that the mesopause altitude at 70°N is around 86 km during the summer and around 100 km during the winter, however Lübken and Müllemann (2003) show that it is somewhat higher up at 89 ± 1.5 km at 78°N, at least in summer. Thus, observations at an altitude of 90 km and 70°N would be from the lower thermosphere in summer and the upper mesosphere in winter. At 78°N, however, observations at 90 km are, to a first approximation, within the mesosphere throughout the whole year. Following Lübken (1996), we can expect little turbulence below the summer mesopause with most energy dissipation occurring in the lowest reaches of the thermosphere. That Ri is, on average, indicative of dynamic stability in this region in summer suggests that turbulence is driven almost exclusively by convective (static) instability. At and immediately above the temperature inversion [described as the steep beach by McIntyre (1989) as mentioned earlier], Brunt-Väisälä periods are short and waves break rapidly, dissipating energy into turbulence. For winter, Lübken (1996) reports less intense turbulence but distributed throughout the mesosphere, and, that our Ri values for winter are indicative of, on average, dynamic instability, is consistent with turbulence driven by a combination of dynamic and static instabilities.

5. Further Interpretation

We have hitherto ascertained that there is a probability that turbulence generation is distributed differently, not only in altitude, but also in mechanism as a function of season. To further investigate the distribution of turbulence generation we have adapted the method of Zink and Vincent (2004) which takes into account the fluctuations in both ω_B and $|d\mathbf{U}/dz|$. Waves, breaking waves and turbulent layers will all induce changes in temperature structure leading to local and temporary perturbations in buoyancy, while waves will directly modulate winds, and perturbations can also be anticipated from momentum deposition. In our formulation of Zink's and Vincent's (2004) approach we do not resolve the wind shear into orthogonal directions but simply define the non-dimensionalized wind shear as:

$$X = \frac{|d\mathbf{U}/dz|}{\omega_B} \tag{5}$$

Zink and Vincent (2004) define Z as the square of the non-dimensionalized instantaneous Brunt-Väisälä frequency,

ω'_B, minus unity:

$$Z = \left(\frac{\omega'_B}{\omega_B}\right)^2 - 1 \tag{6}$$

where ω_B is the mean value as before. Our approach of using ready-averaged ω_B and their standard deviations does not lend itself to this method exactly. We therefore assume Z to have a distribution about zero and to be characterized by a width ΔZ corresponding to the non-dimensionalized variance of ω_B and which is independent of X:

$$\Delta Z = \frac{(\omega_B + \sigma)^2}{\omega_B^2} - 1 \tag{7}$$

where σ is the standard deviation of ω_B. Similarly, ΔX is composed of the standard deviations in both $d\mathbf{U}/dz$ and ω_B. As explained by Zink and Vincent (2004), an atmospheric state mapping onto the region $Z < -1$ is statically unstable; a state mapping onto the region the region $Z > X^2/4 - 1$ is stable; a state mapping onto the region between the abscissa $Z = -1$ and parabola $Z = X^2/4 - 1$ indicates dynamic instability. We now plot the monthly statistics expressed as X, ΔX and ΔZ as rectangles, together with the $Z = -1$ abscissa and $Z = X^2/4 - 1$ parabola (Fig. 11). In Fig. 11, months are arranged in a clockwise fashion with winter at the bottom and summer at the top. Wide rectangles depict large variances in a combination of wind shear and buoyancy; high rectangles depict large fluctuations in buoyancy alone; the position of the rectangle on the X axis indicates Ri (decreasing rightward). It is tempting to determine the percentages of the rectangles falling within each of the states delineated by $Z = -1$ and $Z = X^2/4 - 1$, however we do not wish to take this step and rather present Fig. 11 as a qualitative representation of how turbulence generation changes from month to month. In the winter half of the year we see a tendency towards wide rectangles shifted to large (approx. 1.0) X, suggesting smaller and more fluctuating Ri, while in summer the rectangles are thin and with smaller departures from $X = 0$ indicative of larger Ri and less fluctuation. While the rectangles extend into the static instability region every month, more strongly fluctuating buoyancy is suggested by the rectangles' heights in October and February and, in particular in November. The greatest probability of dynamic instability occurs between November and February. Comparing July with June and August, there is a suggestion of greater buoyancy fluctuation, which if significant could be interpreted as indicative of wave breaking in the lower thermosphere giving rise to increased occurrence of temporary negative ω_B^2. The progression from the well-defined summer mesopause state to a more complicated autumn picture with possible multiple inversion layers as suggested by the temperature profiles presented by Lübken and Müllemann (2003) is consistent with the right-hand side of Fig. 11.

Finally, the most intense turbulence is found to occur at and just above the summer mesopause, and it is here we, prima facie, identify the largest Ri. While shears are less in summer at 90 km, they are not absent and one explanation for larger Ri is that if dynamic instabilities are limited in horizontal extent, they will be smeared out by our spatial averaging. Another explanation is the variation of Ri within turbulent layers (Barat *et al.*, 1997). Perhaps equally likely is that gravity wave breaking dominates the lower thermosphere to such an extent that $0 < \mathrm{Ri} < 0.25$ states cannot persist long enough to contribute to our statistics.

6. Summary

Meteor wind radar echo fading times obtained from 1433 days in the period 2001–2005 are used to determine daily averages of ambipolar diffusion coefficients and then a month-by-month seasonal variation. Subsequent derivation of neutral temperatures including calibration using simultaneous optical measurements (Hall *et al.*, 2004, 2006), allows us to recalibrate the diffusion coefficients and determine their vertical gradients. The recalibrated diffusivities are in good agreement with observations from 43°S and 69°S, suggesting little latitudinal variation. Pressures and their gradients are taken from Lübken (1999) and Lübken and von Zahn (1991), and although really for 70°N, investigation by Holdsworth *et al.* (2006) gives us confidence that they are a good approximation for 78°N. Next, neutral temperature gradients are derived from the above parameters and we identify the transition from positive to negative values in September with the transition from summer to winter mesopause state following Lübken and Müllemann (2003) and consistent with the location of the mesopause with respect to 90 km. Furthermore we note good agreement between our MWR-derived summer temperatures and the results of Lübken and Müllemann (2003). Next, using the temperatures and their gradients we determine monthly average Brunt-Väisälä frequencies (also calculated as periods) and associated monthly variability determined by rigorous propagation of standard deviations from the original measurements. Our confidence in the final results is increased by good agreement with NRLMSIS-00 (Picone *et al.*, 2002) and also agreement with independent measurements of neutral temperature and ambipolar diffusion coefficient in the underlying steps. Apart from the anticipated shorter periods (3.5 ± 3 min) in summer just within the "steep beach" of the lower thermosphere and winter periods around 6 min, there is evidence for occurrences of static instability during most months of the year, and particularly in winter.

In examining wind data at 30 min and 1-km resolutions between 2003 and 2005 inclusive, we have established the presence of a seasonal variation in wind shear at 90 km, 78°N, 16°E, with maxima in winter and minima in summer. Combined with the converse behaviour of the Brunt-Väisälä frequency, we also find a gradient Richardson Number (albeit spatially averaged over the field of view of the radar) seasonal variation indicative of dynamic instability in winter and relative stability in summer; in particular November exhibits more fluctuation in buoyancy than any other month. Taking into account the fluctuations, inferred from monthly standard deviations in wind shear and buoyancy, we deduce that static instability occurs all year round and presumably dominates turbulence generation. Dynamic instability contributes to turbulence in winter, while in summer it is either too short lived to be detected by our approach, or quite simply does not have time to develop in the environment of gravity wave breaking in the base of the lower thermosphere

References

Bertin, F., J. Barat, and R. Wilson, Energy dissipation rates, eddy diffusivity, and the Prandtl number: an in situ experimental approach and its consequences on radar estimate of turbulent parameters, *Radio Sci*., **32**, 791–804, 1997.

Cervera, M. A. and I. M. Reid, Comparison of atmospheric parameters derived from meteor observations with CIRA, *Radio Sci*., **35**, 833–843, 2000.

Fritts, D. C. and M. J. Alexander, Gravity wave dynamics and effects in the middle atmosphere, *Rev. Geophys*., **41**, 1003, doi:10.1029/2001RG000106, 2003.

Galligan, D. P., G. E. Thomas, and W. J. Baggaley, On the relationship between meteor height and ambipolar diffusion, *J. Atmos. Solar-Terr. Phys*., **66**, 899–906, 2004.

Hall, C. M., U.-P. Hoppe, T. A. Blix, E. V. Thrane, A. H. Manson, and C. E. Meek, Seasonal variation of turbulent energy dissipation rates in the polar mesosphere: a comparison of methods, *Earth Planets Space*, **51**, 515–524, 1999.

Hall, C. M., T. Aso, and M. Tsutsumi, An examination of high latitude upper mesosphere dynamic stability using the Nippon/Norway Svalbard Meteor Radar, *Geophys. Res. Lett*., **29**, 1211–1213, 2002.

Hall, C. M., T. Aso, M. Tsutsumi, J. Höffner, and F. Sigernes, Multi-instrument derivation of 90 km temperatures over Svalbard (78°N 16°E), *Radio Sci*., **39**, doi: 10.1029/2004RS003069, 2004.

Hall, C. M., T. Aso, M. Tsutsumi, J. Höffner, F. Sigernes, and D. A. Holdsworth, Neutral air temperatures at 90km and 70° and 78°N, *J. Geophys. Res*., **111**, D14105, doi:10.1029/2005JD006794, 2006.

Holdsworth, D. A., R. J. Morris, D. J. Murphy, I. M. Reid, G. B. Burns, and W. J. R. French, Antarctic mesospheric temperature estimation using the Davis MST radar, *J. Geophys. Res*., **111**, 1–13, D05108, doi:10.1029/2005JD006589, 2006.

Kundu, P. K., *Fluid Mechanics*, 638 pp., Academic Press, San Diego, 1990.

Lübken, F.-J., Rocket-borne measurements of small scale structures and turbulence in the upper atmosphere, *Adv. Space Res*., **17**, (11)25–(11)35, 1996.

Lübken, F.-J., Thermal structure of the Arctic summer mesosphere, *J. Geophys. Res*., **104**, 9135–9149, 1999.

Lübken, F.-J. and A. Müllemann, First in situ measurements in the summer mesosphere at very high latitudes (78°N), *J. Geophys. Res*., **108**(D8), 8448, doi.10.1029/2002JD002414, 2003.

Lübken, F.-J. and U. von Zahn, Thermal structure of the mesopause region at polar latitudes, *J. Geophys. Res*., **96**, 20841–20857, 1991.

McIntyre, M. E., On dynamics and transport near the polar mesopause in summer, *J. Geophys. Res*., **94**, 14617–14628, 1989.

Picone, J. M., A. E. Hedin, D. P. Drob, and A. C. Aikin, NRLMSISE-00 empirical model of the atmosphere: Statistical comparisons and scientific issues, *J. Geophys. Res*., **107**(A12), 1468, doi:10.1029/2002JA009430, 2002.

Roper, R. G. and J. W. Brosnahan, Imaging Doppler interferometry and the measurement of atmospheric turbulence, *Radio Sci*., **32**, 1137–1148, 1997.

Singer, W., J. Bremer, J. Weiß, W. K. Hocking, J. Höffner, M. Donner, and P. Espy, Meteor radar observations at middle and Arctic latitudes, Part 1: mean temperatures, *J. Atmos. Solar-Terr. Phys*., **66**, 607–616, 2004.

Weinstock, J., Vertical turbulent diffusion in a stably stratified fluid, *J. Atmos. Sci*., **35**, 1022–1027, 1978.

Zink, F. and R. A. Vincent, Some inferences on turbulence generation by gravity waves, *J. Geophys. Res*., **109**, doi:10.1029/2003JD003992, 2004.

C. M. Hall (e-mail: Chris.Hall@tgo.uit.no), T. Aso, and M. Tsutsumi